Solution Properties of a Fluorinated Alkyl Methacrylate Polymer in Carbon Dioxide

ARTICLE *in* MACROMOLECULES · MAY 2006

Impact Factor: 5.8 · DOI: 10.1021/ma052409k

Solution Properties of a Fluorinated Alkyl Methacrylate Polymer in Carbon Dioxide

Ji Guo,[†] Pascal André,[†] Mireille Adam,[†] Sergey Panyukov,[†,§] Michael Rubinstein,*[,†] and Joseph M. DeSimone*[,†,‡]

Department of Chemistry, University of North Carolina at Chapel Hill, Chapel Hill, North Carolina 27599-3290; Department of Chemical and Biomolecular Engineering, North Carolina State University, Raleigh, North Carolina 27695-7905; and P. N. Lebedev Physics Institute, Russian Academy of Sciences, Moscow 117924, Russia

Received November 11, 2005; Revised Manuscript Received March 8, 2006

ABSTRACT: The solution properties of a fluorinated alkyl methacrylate, poly(1,1,2,2-tetrahydroperfluorooctyl methacrylate) (PFOMA), in liquid and supercritical carbon dioxide (CO_2) were studied by static and dynamic light scattering. The solvent quality of CO_2 was found to improve with increasing temperature and CO_2 density as exhibited by an increase of the second virial coefficient. Both the hydrodynamic radius expansion factor and the second virial coefficient of PFOMA solution were found to be functions of a single interaction parameter that can be independently changed by either temperature or density variations. Furthermore, we demonstrate that the relationship between two directly measurable quantities, the second virial coefficient and the hydrodynamic expansion ratio, is the same for both temperature-induced and CO_2 density-induced variations of solvent quality.

I. Introduction

As a solvent, supercritical carbon dioxide ($scCO_2$) possesses many unique characteristics including an easily accessible critical point[1] (a critical temperature, T_c, of 31.1 °C and a critical pressure, p_c, of 73.8 bar).[2] A unique feature of $scCO_2$ is the ability to easily tune the solvent quality by changing the temperature (T) or CO_2 density (ρ).[3] Many amorphous fluoropolymers are soluble in liquid or supercritical carbon dioxide.[1,4] The ability to dissolve polymers in $scCO_2$ creates new opportunities in chemical manufacturing, such as spin-coating and spray-coating from liquid CO_2, separations, and complexation of organic acids and heavy metals.[5−13] Therefore, it is necessary to understand the solvent properties of CO_2 for the various polymers envisaged for these applications.

Various experimental techniques have been used to characterize polymer solutions in carbon dioxide.[14−19] The most commonly used method to characterize polymer solubility in a supercritical fluid is to perform phase equilibrium measurements to determine cloud point curves as a function of temperature or CO_2 density at a given polymer concentration.[20] Recently, high-pressure scattering methods have been used for quantitative measurements of polymer solution behavior to get information about interactions and molecular sizes in carbon dioxide.[21−23]

In this work, we study the influence of solvent density and temperature on the properties of a fluorinated poly(alkyl methacrylate), PFOMA, in CO_2. We investigate the change of solvent quality using two different approaches, as shown in Figure 1: (1) by varying the temperature at a constant CO_2 density; (2) by changing CO_2 density at a constant temperature. Using high-pressure static and dynamic light scattering, we measured the molecular weights and sizes of fractionated PFOMA samples. The second virial coefficient and hydrodynamic radius were found to increase with increasing temperature and CO_2 density. The focus of this work was to construct functions of a single interaction parameter which enable one to quantitatively predict the strength of interactions and sizes of PFOMA in CO_2 with the change of temperature or solvent density for different PFOMA molecular weights. For example, one can use this function to calculate how to tune the temperature and CO_2 density to get a desired polymer size or interaction parameter. We demonstrate that both the second virial coefficient and the hydrodynamic radius expansion coefficient can be expressed as functions of a single interaction parameter z that varies with temperature (T) at constant CO_2 density (ρ) as $N^{1/2}[1 - \theta(\rho)/T]$ and with CO_2 density at constant temperature as $N^{1/2}[1 - \rho_\theta(T)/\rho]$, where $\theta(\rho)$ is the theta temperature for given density ρ, ρ_θ is the theta density (the CO_2 density at the theta condition), and N is the number of Kuhn segments of the polymer chains. The relationship between the second virial coefficient (A_2) and the hydrodynamic radius expansion factor (α_h) was found to follow the same behavior (independent of directions in Figure 1). Therefore, we verified that two different ways of varying the interaction parameter z (directions (1) and (2) in Figure 1) are directly related and found that the θ-temperature varies reciprocally proportional to CO_2 density

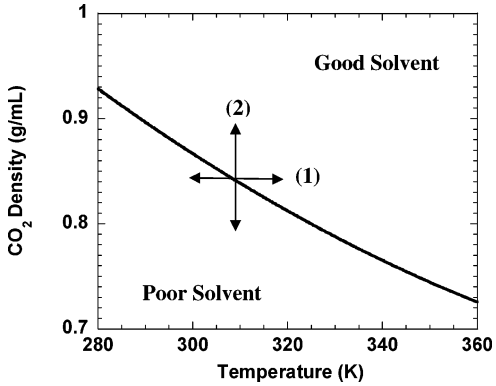

Figure 1. Theta curve (dependence of θ-density on θ-temperature) for PFOMA solution in CO_2.

[†] University of North Carolina at Chapel Hill.
[‡] North Carolina State University.
[§] Russian Academy of Sciences.
* To whom correspondence should be addressed: e-mail mr@unc.edu, desimone@unc.edu.

10.1021/ma052409k CCC: $33.50
Published on Web 04/08/2006

$\theta(\rho) = (260/\rho)(KmL/g)$, while the θ-density varies reciprocally proportional to the absolute temperature $\rho_\theta(T) = (260/T)$(g K/mL). Thus, we have confirmed the existence of a single interaction parameter that combines the temperature, the solvent density, and the degree of polymerization into a single variable.

II. Experimental Section

II.1. Materials. The monomer 1,1,2,2-tetrahydroperfluorooctyl methacrylate (FOMA) (provided by DuPont) was purified and deinhibited by passing it through an alumina column. The initiator 2,2′-azobis(isobutyronitrile) (AIBN, Kodak, 99%) was recrystallized twice in methanol (Aldrich). All purification solvents were purchased from Aldrich and used as received.

II.2. Synthesis of PFOMA. FOMA monomers were purged with argon for ~15 min prior to transferring into a 25 mL high-pressure view cell containing AIBN (0.5−1 wt %) and a magnetic stirring bar. The contents of the high-pressure cell were purged with argon for additional 15 min, and then the reaction cell was heated to 60 °C while CO_2 was added via syringe pump (Isco) over ca. 15 min of time to a pressure of 345 bar. The polymerization was continued for 24 h at 60 °C and 345 bar. The resulting polymer and any unreacted monomer were removed from the reaction cell by dissolving all of the contents in 1,1,2-trifluorotrichloroethane. The polymer was precipitated into a large excess of methanol, isolated by suction filtration, washed several times with methanol, and dried in a vacuum oven overnight under reduced pressure.

II.3. Fractionation and Preparation of Polymer Solutions. The isolated PFOMA was fractionated to reduce the polydispersity of samples used in the analysis. Under isothermal conditions, PFOMA was fractionated by applying an increasing CO_2 pressure profile.[3] The fractionation temperature was 60 °C, and the pressure was increased from 106 to 414 bar with a step interval of 14 bar. A total of 13 fractions were isolated at different CO_2 densities. Each fraction was 1.5−2 g in mass and was numbered consecutively from 1 to 13. Fractions 2 and 8 were used to measure the refractive index, and fractions 3 and 6 were used to do all other measurements.

The concentration of the polymer solutions used in the light scattering experiments ranged from 0.01 to 0.04 g/mL. The polymer samples were weighed and sealed into a high-pressure optical cell (see details in the Supporting Information). The cell volume was adjusted using a piston at the top of the optical cell. Carbon dioxide was filtered and injected slowly into the cell at room temperature, until the initial pressure reached 131 bar. The polymer solution was then heated to 60 °C with constant stirring until it became completely transparent. Subsequently, the solution was stabilized without stirring for 1.5 h while the transmission intensity of the polymer solution was detected using a LaserPAD power meter (Coherent Inc.). All experimental conditions were reached by decreasing temperatures and/or by increasing the CO_2 density. The scattering intensity was monitored by a photometer with each temperature and density change until the intensity became stable.

II.4. Measurement of Refractive Index Increment. The refractive index increment (dn/dc) quantifies how the refractive index of the polymer solution changes with polymer concentration. For traditional solvents, dn/dc is measured with a differential refractometer, and the values for many systems are available in the literature.[24] The values of dn/dc for most polymers in CO_2, however, are unknown and needed to be measured directly. The measurements of the refractive index increment of two fractions of PFOMA in CO_2 are described in the Supporting Information.

II.5. Light Scattering. Static light scattering (SLS) and dynamic light scattering (DLS) experiments were performed by means of a spectrometer equipped with an argon laser (see the Supporting Information). The scattering wave vector q is given by

$$q = \frac{4\pi n_s}{\lambda}\sin(\Theta/2) \tag{1}$$

where n_s is the refractive index of the solvent, λ is the wavelength of the light in the vacuum, and Θ is the scattering angle.[25] The refractive index values n_s for carbon dioxide were measured under experimental conditions. The range of the external detection angle was varied from 25° to 155°, which results in a scattering wavevector q that ranged from 0.010 to 0.027 nm^{-1}. All DLS experiments were performed at angles 40°, 90°, and 140°.

Table 1. Rayleigh Ratios $R_\theta^{CO_2}$ of CO_2 at Scattering Angle 90° for Different CO_2 Densities at 25 °C

CO_2 density (g/mL)	0.86	0.89	0.93	0.97	1.01
$R_\theta^{CO_2} \times 10^5$ (cm^{-1})	3.87	3.37	2.75	2.26	1.97

II.5.1. Static Light Scattering. Static light scattering experiments measure the relative excess of scattering intensity with respect to the solvent $I(q,c)$ for various polymer concentrations and $I(q,c) = (I_s - I_{CO_2})/I_{CO_2}$, where the I_s and I_{CO_2} are the scattering from the polymer solution and from CO_2, respectively. The scattering data were converted into the excess Rayleigh's ratio, $R(q,c)$, using the equation[26] $R(q,c) = I(q,c)R_\theta^{CO_2} = I(q,c)R_\theta^{toluene}I_{CO_2}/I_{toluene}$. The Rayleigh ratio of toluene is $R_\theta^{toluene} = 3.21 \times 10^{-5}$ cm^{-1} at 25 °C for $\lambda = 514$ nm, and the Rayleigh ratios of CO_2 ($R_\theta^{CO_2}$) at 25 °C are listed in Table 1.

The dependence of the excess Rayleigh ratio $R(q,c)$ on scattering wavevector q and polymer concentration c is expressed as[26]

$$\frac{Kc}{R(q,c=0)} = \frac{1}{M_w}\left(1 + \frac{1}{3}R_g^2q^2...\right) \tag{2}$$

$$\frac{Kc}{R(q=0,c)} = \frac{1}{M_w}(1 + 2M_wA_2c...) \tag{3}$$

Here A_2 is the second virial coefficient, R_g is the z-average radius of gyration, and M_w is the weight-average molecular weight. The optical constant K is defined by[26]

$$K = \frac{4\pi^2n_s^2}{\lambda^4N_{av}}\left(\frac{dn}{dc}\right)^2 \tag{4}$$

where N_{av} is Avogadro's number.

II.5.2. Dynamic Light Scattering. Dynamic light scattering (DLS) measures the autocorrelation function $g^{(2)}(q,t)$ of the scattering intensity.[26] The autocorrelation function depends on how molecules move on the length scale $1/q$, with a characteristic time

$$\tau = \frac{1}{Dq^2} \tag{5}$$

where D is the diffusion coefficient. For dilute solutions, the concentration dependence of the diffusion coefficient $D(c)$ can be approximated as[27]

$$D(c) = D_0(1 + k_Dc) \tag{6}$$

where k_D is the diffusional second virial coefficient and D_0 is the diffusion coefficient at infinite dilution

$$D_0 = \frac{k_BT}{6\pi\eta_sR_h} \tag{7}$$

where η_s is the solvent viscosity, k_B is the Boltzmann constant, T is the absolute temperature, and R_h is the hydrodynamic radius. Equation 7 is used to calculate hydrodynamic radius R_h from the diffusion coefficient D_0 obtained by extrapolation of D(c) (eq 6) to infinite dilution ($c \rightarrow 0$).

II.6. Interaction Parameter. The second virial coefficient of polymers dissolved in organic solvents can be collapsed onto a single curve without any adjustable parameters as was first demonstrated by Berry for polystyrene solutions.[28] In a good solvent

Table 2. Mass of Kuhn Segment M_s and Kuhn Length b of PFOMA, PMMA,[30] and PS[28]

polymer	M_s (Da)	b (nm)
PFOMA	6300	3.0
PMMA	666	1.7
PS	728	1.8

and in a θ-region,[29] $A_2M_w^{1/2}$ is only a function of chain interaction parameter, z.

$$A_2M_w^{1/2}\frac{M_0^{3/2}}{N_{av}b^3} = f(z) \approx C^{A_2}\begin{cases} z & \text{for } |z| < 1 \quad (\theta \text{ region}) \\ z^{0.528} & \text{for } z > 1 \quad \text{(good solvent)} \end{cases} \tag{8}$$

where C^{A_2} is a numerical coefficient. Kuhn segment mass, M_s, and length, b, are defined through the equivalent freely jointed chain model.[29]

$$b = \frac{6R_{g\theta}^2}{l}\frac{m_s}{M_w} \tag{9}$$

$$M_s = 6\left(\frac{R_{g\theta}m_s}{l}\right)^2\frac{1}{M_w} \tag{10}$$

where m_s is the molar mass of the monomer, $R_{g\theta}$ is the radius of gyration at the θ-condition, and the contour length of the monomer is $l = 2 \times 1.54$ Å $\times \sin(68°) = 2.6$ Å. The length b and the mass M_s of the Kuhn segment for PFOMA (see section IV.2), polystyrene (PS),[28] and poly(methyl methacrylate) (PMMA)[30] are listed in Table 2.

The interaction parameter z at constant solvent density can be expressed in terms of the reduced temperature (see direction (1) in Figure 1)

$$z = C_TN^{1/2}\frac{T-\theta(\rho)}{T} \quad (\rho = \text{const}) \tag{11}$$

where C_T is a numerical coefficient related to the temperature dependence of interaction parameter z and N is the number of Kuhn segments, $N = M_w/M_0$. Similarly, the interaction parameter z at constant temperature can be expressed in terms of the reduced density (see direction (2) in Figure 1)

$$z = C_\rho N^{1/2}\frac{\rho-\rho_\theta(T)}{\rho} \quad (T = \text{const}) \tag{12}$$

where C_ρ is a numerical coefficient related to the density dependence of the interaction parameter z. In section IV.3 we present a theoretical analysis of the temperature and density dependencies of the second virial coefficient in supercritical solvents and derive the temperature dependence of the theta density $\rho_\theta(T)$. Numerical coefficients C^{A_2}, C_T, and C_ρ can depend on chemical structure of polymer. For a particular polymer−solvent pair, these coefficients should be independent of molecular weight, and we will demonstrate below that C_T and C_ρ are equal to each other for PFOMA in CO_2.

In the θ-region, the second virial coefficient is linearly proportional to the interaction parameter z (see eq 8 with eq 11 for temperature variations and eq 12 for density variations).

$$A_2M_w^{1/2}\frac{M_0^{3/2}}{N_{av}b^3} = C^{A_2}z = \begin{cases} C_T^{A_2}N^{1/2}\left[1-\dfrac{\theta(\rho)}{T}\right] & \text{for temperature variations} \quad (C_T^{A_2} = C^{A_2}C_T) \\ C_\rho^{A_2}N^{1/2}\left[1-\dfrac{\rho_\theta(T)}{\rho}\right] & \text{for density variations} \quad (C_\rho^{A_2} = C^{A_2}C_\rho) \end{cases} \tag{13}$$

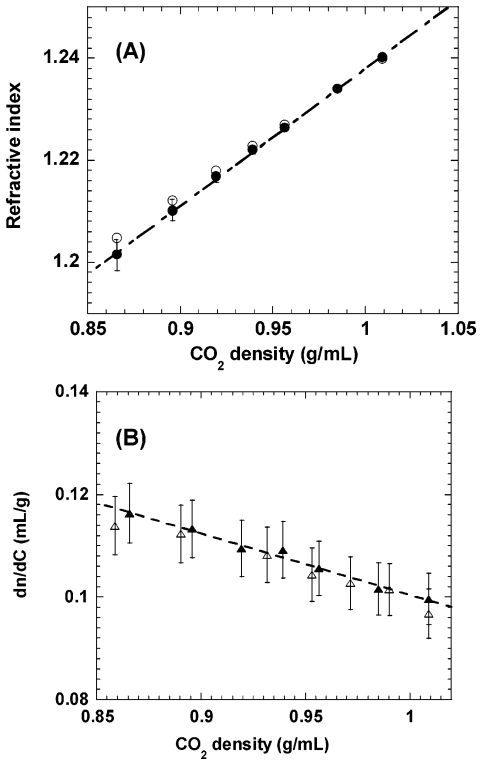

Figure 2. (A) Refractive index of carbon dioxide as a function of CO_2 density at 25 °C: values calculated from ref 32 (○) and our measurements (●). (B) dn/dc as a function of CO_2 density at 25 °C for two PFOMA fractions: fraction 2 (△) and fraction 8 (▲).

The hydrodynamic radius expansion factor α_h is defined as the ratio of hydrodynamic radius R_h at a given condition to the hydrodynamic radius at the θ-condition, $R_h(\theta)$. This expansion ratio α_h, describing the swelling of the chain, is also a function of a single interaction parameter z[27,31] (related to the excluded volume interactions). The hydrodynamic radius expansion factor α_h can be approximated in the θ-region by a linear function of the interaction parameter z.[32]

$$\alpha_h = 1 + C^Rz = \begin{cases} 1 + C_T^RN^{1/2}\left[1-\dfrac{\theta(\rho)}{T}\right] & \text{for temperature variations} \quad (C_T^R = C^RC_T) \\ 1 + C_\rho^RN^{1/2}\left[1-\dfrac{\rho_\theta(T)}{\rho}\right] & \text{for density variations} \quad (C_\rho^R = C^RC_\rho) \end{cases} \tag{14}$$

where C^R is a numerical coefficient. Furthermore, the existence of a single interaction parameter for both temperature and density variations implies that these coefficients are not independent, but are related to each other by

$$\frac{C_T^R}{C_T^{A_2}} = \frac{C^R}{C^{A_2}} = \frac{C_\rho^R}{C_\rho^{A_2}} \tag{15}$$

as can be deduced from eqs 13 and 14.

III. Results

III.1. Molecular Weight M_w. The measurements of the refractive index and the static light scattering experiments were carried out in order to determine the molecular weights of the various PFOMA fractions. The values of refractive index of carbon dioxide calculated from the literature[25] have been confirmed in our experiments, as shown in Figure 2A. The refractive index values of carbon dioxide were found to increase linearly with CO_2 density. The values of the refractive index

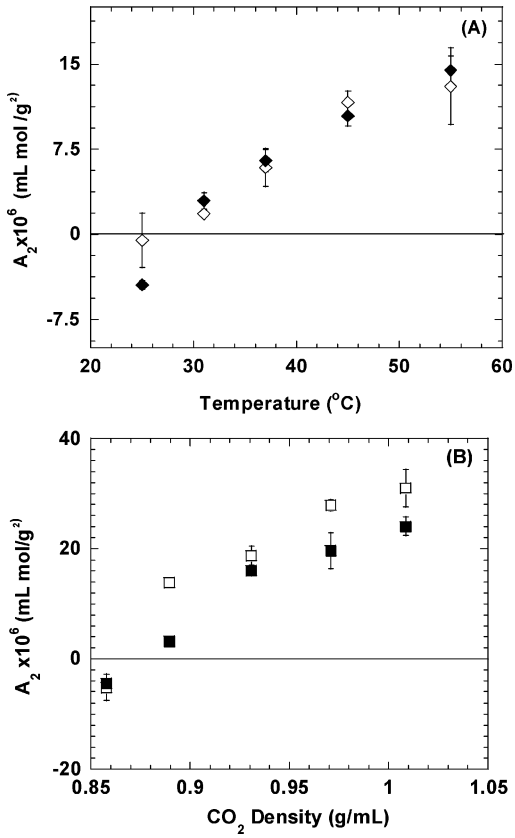

Figure 3. Variation of the second virial coefficient A_2 with (A) temperature at constant CO_2 density $\rho = 0.86$ g/mL, PFOMA with $M_w = 300$ kDa (◇) and $M_w = 900$ kDa (◆); (B) CO_2 density at constant temperature $T = 25$ °C, PFOMA with $M_w = 300$ kDa (□) and $M_w = 900$ kDa (■).

increments (d*n*/d*c*) at different CO_2 densities at 25 °C for two PFOMA fractions (fractions 2 and 8) are displayed in Figure 2B. As the carbon dioxide density increases, the d*n*/d*c* values for both fractions of PFOMA in CO_2 decrease from 0.12 to 0.10 mL/g. The effect of CO_2 density on the d*n*/d*c* of the polymer solutions can be mostly attributed to the change of CO_2 refractive index with CO_2 density (see Supporting Information). The d*n*/d*c* values are independent of PFOMA molecular weight, as expected for long polymeric chains where the end groups have negligible effects on the polymer solution properties. The data for fractions 2 and 8 at the same CO_2 density agree with each other within experimental accuracy.

The molecular weights of fractions 3 and 6 were measured by light scattering using d*n*/d*c* values determined from fractions 2 and 8. The molecular weights of fractions 3 and 6 were found to be 300 ± 30 and 900 ± 70 kDa, respectively.

III.2. Second Virial Coefficient A_2. The solvent quality change can be monitored through measurements of A_2 at different temperatures and solvent densities of CO_2. The second virial coefficient, A_2, was determined from the concentration dependence of the scattering intensity from dilute PFOMA solutions. The temperatures and densities corresponding to θ-conditions with the second virial coefficient equal to zero can be determined at constant density by varying the temperature (direction (1) in Figure 1) or at constant temperature by varying the density (direction (2) in Figure 1). Previous small-angle neutron scattering experiments have demonstrated that not only does a θ-temperature but a θ-density can also exist for a CO_2−polymer solution.[33]

When the CO_2 density was kept constant (0.86 g/mL), A_2 was found to increase with increasing temperature (Figure 3A), changing from negative to positive values. In the range of experimental conditions investigated, the PFOMA samples with both molecular weights (300 and 900 kDa) had the same θ-point [$\theta = 27 \pm 1$ °C, $\rho_\theta = 0.86$ g/mL]. The variation of A_2 with carbon dioxide density at constant temperature (25 °C) is displayed in Figure 3B. A_2 was found to increase with increasing density, ranging from negative to positive values. The increase of the second virial coefficient with density is stronger for the lower molecular weight fraction. The θ-condition was determined to be [$\theta = 25$ °C, $\rho_\theta = 0.88 \pm 0.02$ g/mL]. The improvement of the solvent quality quantitatively assessed by static light scattering was confirmed by the variation of the diffusional second virial coefficient k_d deduced from the dynamic light scattering data (see Supporting Information).

III.3. Size Variations of Polymer Chains. The radius of gyration of the fraction with $M_w = 900$ kDa is $R_g = 15 \pm 4$ nm, at θ-conditions [$\theta = 27 \pm 1$ °C, $\rho(\theta) = 0.86$ g/mL] and [$\theta = 25$ °C, $\rho(\theta) = 0.88 \pm 0.02$ g/mL]. There was no measurable change of R_g within the experimental error with variations of either CO_2 density or temperature (see Figure SI-4 in Supporting Information). For the fraction with $M_w = 300$ kDa, the radius of gyration could not be measured by static light scattering. The values of R_g for PFOMA with $M_w = 900$ kDa are close to the detection limit of our instrument. The difficulty of the measurements of R_g for the high molecular weight sample is clearly displayed in the plot of $c/I(q,c) \sim q^2$ (see Figure SI-3B in the Supporting Information). The contrast between the polymer and supercritical CO_2 is much lower than the contrast in organic systems.

The hydrodynamic radius R_h was measured by the dynamic light scattering. The hydrodynamic radii R_h at θ-conditions [$\theta = 27 \pm 1$ °C, $\rho_\theta = 0.86$ g/mL] and [$\theta = 25$ °C, $\rho_\theta = 0.88 \pm 0.02$ g/mL] are 6.4 ± 0.1 and 11.4 ± 0.2 nm for the low (300 kDa) and the high (900 kDa) molecular weight fractions (fractions 3 and 6), respectively. The ratio of R_g/R_h for the sample with molecular weight 900 kDa was found to be 1.3 ± 0.4 at θ-conditions, which is very close to the value reported for monodisperse linear polymers.[29] Figure 4 illustrates the dependence of hydrodynamic radius expansion ratio α_h on temperature (A) and CO_2 density (B). The values of α_h increase with increasing temperature and CO_2 density. This observation verifies that the polymer size increases with the improvement of solvent quality along both the temperature and density directions (see Figure 1). The increase of hydrodynamic radius expansion factor with temperature or density is stronger for the higher molecular weight fraction.

IV. Discussion

IV.1. Hydrodynamic Radius. It is demonstrated in Figure 5A that the hydrodynamic radius expansion factor for different polymer solutions can be expressed as the universal function of the reduced temperature $N^{1/2}[1 - \theta(\rho)/T]$ (eq 14), including the data for PFOMA in CO_2 and the data from earlier experiments on polystyrene (PS) in two different solvents.[32,34] In the θ-region, α_h is approximately a linear function of reduced temperature $N^{1/2}[1 - \theta(\rho)/T]$, and the numerical coefficient C_T^R is 0.06 ± 0.01 for both PFOMA in CO_2 and polystyrene in organic solvents.[32,34,35] The radius of gyration expansion factor α_g (defined as the ratio of R_g at a given condition to the radius of gyration $R_{g\theta}$ at the θ-point) is also a universal function of reduced temperature $N^{1/2}[1 - \theta(\rho)/T]$.[28,36] The earlier experimental results for PS[32,34] and PMMA[37] in different organic solvents also exhibit the linear relationship between α_g and reduced temperature in the θ-region that can be written as α_g

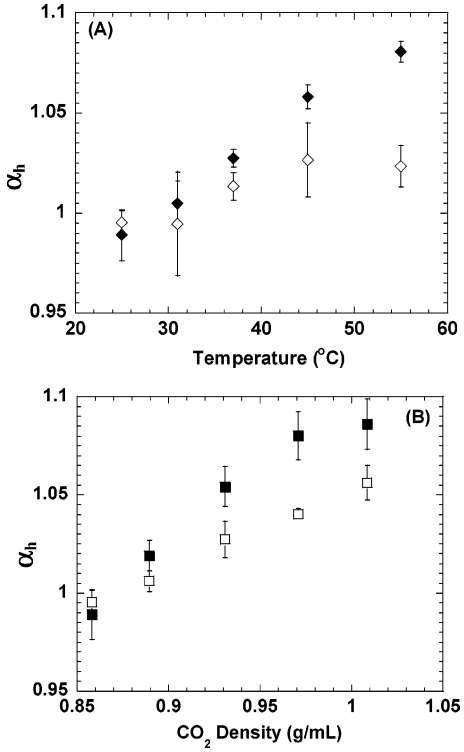

Figure 4. Hydrodynamic expansion factor α_h: (A) as a function of temperature at constant CO_2 density of $\rho = 0.86$ g/mL, PFOMA with $M_w = 300$ kDa (◇) and $M_w = 900$ kDa (◆); (B) as a function of CO_2 density at constant temperature $T = 25$ °C. PFOMA with $M_w = 300$ kDa (□) and $M_w = 900$ kDa (■).

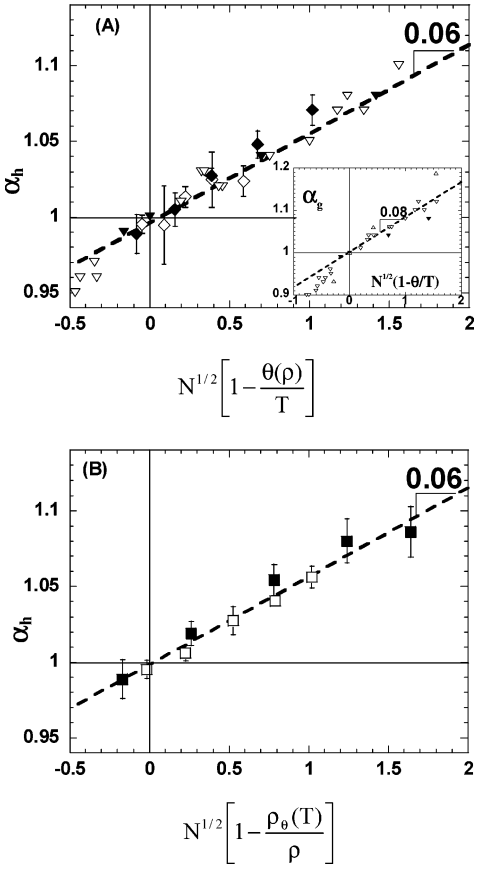

Figure 5. (A) Hydrodynamic radius expansion factor α_h as a function of the reduced temperature $N^{1/2}[1 - \theta(\rho)/T]$ at constant CO_2 density $\rho = 0.86$ g/mL with $\theta(\rho) = 27$ °C, for PFOMA with $M_w = 300$ kDa (◇) and $M_w = 900$ kDa (◆), PS in cyclohexane[32] (▽), PS in *trans*-decalin[34] (▼). Inset: radius of gyration expansion factor $\alpha_g = R_g/R_g(\theta)$ as a function of the chain interaction parameter $N^{1/2}(1 - \theta/T)$, for PS in cyclohexane[32] (▽), PS in *trans*-decalin[34] (▼), PMMA in water and *tert*-butyl alcohol[37] (△). (B) Hydrodynamic radius expansion ratio α_h as a function of the reduced density $N^{1/2}[1 - \rho_\theta(T)/\rho]$ at constant temperature $T = 25$ °C with $\rho_\theta = 0.88$ g/mL, for PFOMA with $M_w = 300$ kDa (□) and $M_w = 900$ kDa (■).

$= 1 + (0.08 \pm 0.02)N^{1/2}(1 - \theta/T)$ (the inset in Figure 5A). The coefficients C_T^R for hydrodynamic radius expansion factor α_h and for the radius of gyration expansion factor α_g of PS in *trans*-decalin are equal to each other within experimental error, as expected from the fact that the ratio of R_g/R_h should not have significant temperature dependence in the θ-region. It is interesting to note that numerical coefficients C_T^R for different polymers (PFOMA, PS, and PMMA) are close to each other.

We observe for the first time that polymer size is a function of the reduced solvent density $N^{1/2}[1 - \rho_\theta(T)/\rho]$ (direction (2) in Figure 1). There is a linear relationship between the hydrodynamic radius expansion factor α_h and the reduced density in the θ-region (see Figure 5B and eq 14), and the numerical coefficient $C_\rho^R = 0.06 \pm 0.01$ turned out to be equal to C_T^R within the experimental accuracy.

IV.2. Second Virial Coefficient. It was reported that experimental data as well as computer simulation data for the second virial coefficient of different polymers (e.g., polystyrene[28] and poly(methyl methacrylate)[30]) in various organic solvents can be expressed as functions of the interaction parameter $z \sim N^{1/2}(1 - \theta/T)$ (see eq 13). The dependence of the normalized second virial coefficient on the reduced temperature $N^{1/2}[1 - \theta(\rho)/T]$ of PFOMA solutions in CO_2 is presented in Figure 6A. The data of PFOMA samples for both molecular weights collapse onto a single curve. Most of the PFOMA points are in θ-region, where the interaction parameter is small and the dependence of normalized second virial coefficient on reduced temperature $N^{1/2}[1 - \theta(\rho)/T]$ is linear. The numerical coefficient for the θ-region of PFOMA solution in CO_2 is $C_T^{A_2} = 0.50 \pm 0.05$ (eq 13), which is larger than the coefficients 0.39 ± 0.04 for PS and PMMA in organic solvents (shown in the inset in Figure 6A). This difference in coefficients is probably due to different chemical structures of the polymers: the PFOMA has larger Kuhn segment than PS and PMMA (see Table 1).

In a compressible solvent like CO_2, the interaction parameter can be easily varied by changing the solvent density. The behavior of the second virial coefficients as a function of reduced density $N^{1/2}[1 - \rho_\theta(T)/\rho]$ is presented in Figure 6B. The data for two different molecular weight fractions of PFOMA collapse onto a single curve similar to the curve in Figure 6A. This is the first demonstration that the second virial coefficient A_2 of polymers in compressible solvents is a function of the single interaction parameter $z \sim N^{1/2}[1 - \rho_\theta(T)/\rho]$. The numerical coefficient of the linear dependence of the normalized second virial coefficient on the reduced density $N^{1/2}[1 - \rho_\theta(T)/\rho]$ for the θ-region is $C_\rho^{A_2} = 0.50 \pm 0.05$ (eq 13), which is equal to the value of coefficient $C_T^{A_2}$ within experimental error. The ratios of numerical coefficients for the temperature variation ($C_T^R/C_T^{A_2} = C^R/C^{A_2} \cong 0.12$) and for the density variation ($C_\rho^R/C_\rho^{A_2} = C^R/C^{A_2} \cong 0.12$) are equal to each other, as expected from eq 15.

The plots in Figures 5 and 6 are based on assumptions that the interaction parameter is a linear function of either reduced temperature or reduced density. To combine solvent quality changes with both temperature and density variations (both directions in Figure 1), the dependence of hydrodynamic radius

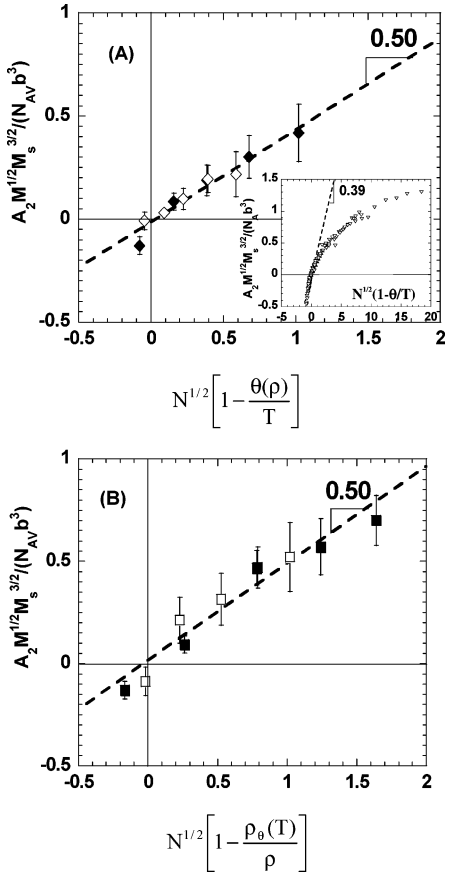

Figure 6. (A) Plot of $A_2M^{1/2}M_s^{3/2}N_{AV}{}^{-1}b^{-3}$ as a function of reduced temperature $N^{1/2}[1-\theta(\rho)/T]$ at constant CO_2 density $\rho_{CO_2} = 0.86$ g/mL with $\theta(\rho) = 27$ °C, of PFOMA with $M_w = 300$ kDa (◇) and $M_w = 900$ kDa (◆). Inset: the plot of $A_2M^{1/2}M_s^{3/2}N_{AV}{}^{-1}b^{-3}$ as a function of reduced temperature $N^{1/2}(1-\theta/T)$ for PMMA in 46.8% butanol/53.2% 2-propanol[30] (▽) and PS in decalin[28] (▼). (B) Plot of $A_2M^{1/2}M_s^{3/2}N_{AV}{}^{-1}b^{-3}$ as a function of reduced density $N^{1/2}[1-\rho_\theta(T)/\rho]$ at constant temperature $T = 25$ °C with $\rho_\theta = 0.88$ g/mL, PFOMA with $M_w = 300$ kDa (□) and $M_w = 900$ kDa (■).

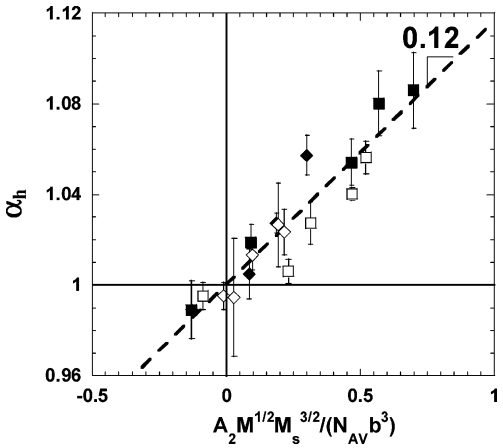

Figure 7. Plot of the hydrodynamic radius expansion factor α_h as a function of $A_2M^{1/2}M_s^{3/2}N_{AV}{}^{-1}b^{-3}$: PFOMA at constant temperature $T = 25$ °C with $\rho_\theta = 0.88$ g/mL, of PFOMA with $M_w = 300$ kDa (□) and $M_w = 900$ kDa (■); PFOMA at constant CO_2 density $\rho_{CO_2} = 0.86$ g/mL with $\theta(\rho) = 27$ °C, of PFOMA with $M_w = 300$ kDa (◇) and $M_w = 900$ kDa (◆).

expansion factor α_h on the second virial coefficient $A_2M^{1/2}M_s{}^{3/2}N_{av}{}^{-1}b^{-3}$ has been plotted in Figure 7 for PFOMA at different CO_2 densities and temperatures. In the experimental range, the PFOMA data collapsed onto a single curve with the slope $C^R/C^{A_2} = 0.12 \pm 0.02$. The hydrodynamic radius expansion factor of PFOMA in CO_2 can be approximated in the θ-region by a linear function of the second virial coefficient.

$$\alpha_h = 1 + \frac{C^R}{C^{A_2}} A_2 M_w{}^{1/2} \frac{M_0{}^{3/2}}{N_{av}b^3} = 1 + (0.12 \pm 0.02) A_2 M_w{}^{1/2} \frac{M_0{}^{3/2}}{N_{av}b^3} \quad (16)$$

The data of PS and PMMA also collapse onto a single curve but with a higher slope of 0.2 ± 0.03. These curves provide a more direct way of predicting the interactions and polymer size in solutions, either getting size information from interactions or obtaining interactions information from polymer size, since both A_2 and α_h can be measured directly and independently by the light scattering experiments.

IV.3. Theta Curve. We independently verified that numerical coefficients $C_T{}^R$ and $C_\rho{}^R$ are equal to each other (see Figure 5) and numerical coefficients $C_T{}^{A_2}$ and $C_\rho{}^{A_2}$ are equal to each other (see Figure 6). Thus, we have two independent verifications that coefficients C_T and C_ρ in eqs 11 and 12 are the same, since these two equations are two different representations of the same interaction parameter z. We conclude that $\theta\rho_\theta =$ constant and the density dependence of θ-temperature is

$$\theta(\rho) = \frac{260}{\rho}\left(\frac{gK}{mL}\right) \quad (17)$$

while the temperature dependence of θ-density is

$$\rho_\theta(T) = \frac{260}{T}\left(\frac{KmL}{g}\right) \quad (18)$$

Below we present a theoretical justification of the hyperbolic CO_2 density dependence of θ-temperature (Figure 1).

In highly compressible solvents (such as CO_2 near its critical point), the second virial coefficient of interaction between solvent molecules is small, and the free energy density of the solvent is dominated by the third virial term

$$F_{CO_2} \approx \frac{B_3\rho^3}{3} \quad (19)$$

where B_3 is solvent interaction parameter. There are additional interaction terms in free energy density of a polymer solution with Kuhn segment number density c_k in this compressible solvent: a term proportional to $\rho_{CO_2}c_k$ due to polymer−solvent interaction and a term proportional to $c_k{}^2$ due to direct polymer−polymer interaction

$$F \approx \frac{B_3\rho^3}{3} + B_2\rho c_k + k_B T\nu\frac{c_k{}^2}{2} \quad (20)$$

where B_2 is the polymer−solvent interaction parameter, k_B is the Boltzmann constant, and ν is the excluded volume of monomers. Because of small interval of temperature variations, we neglect temperature dependences of the interaction parameters B_2 and B_3.

To take into account the density fluctuation of a compressible solvent, we can write the local density ρ as a sum of an average density $\bar{\rho}$ and a density fluctuation $\delta\rho$

$$\rho = \bar{\rho} + \delta\rho \quad (21)$$

Substituting this expression into free energy density (eq 20) and expanding it to quadratic terms in density fluctuation, we find

$$F \approx \frac{B_3\bar{\rho}^3}{3} + B_3\bar{\rho}^2\delta\rho + B_3\bar{\rho}(\delta\rho)^2 + B_2\bar{\rho}c_k + B_2c_k\delta\rho + k_BT\nu\frac{c_k^2}{2} \quad (22)$$

The sum of density fluctuations over the solution volume is zero, $\int_V \delta\rho \, dV = 0$, and therefore the second term in eq 22 vanishes. Note that linear term in solvent density fluctuation $B_2c_k\delta\rho$ does not vanish because the polymer concentration c_k fluctuates in a correlated way with solvent density. Minimizing the free energy density

$$F \approx \frac{B_3\bar{\rho}^3}{3} + B_3\bar{\rho}(\delta\rho)^2 + B_2\bar{\rho}c_k + B_2c_k\delta\rho + k_BT\nu\frac{c_k^2}{2} \quad (23)$$

with respect to the solvent density fluctuation $\delta\rho$

$$\frac{\partial F}{\partial(\delta\rho)} = 2B_3\bar{\rho}\delta\rho + B_2c_k = 0 \quad (24)$$

we find the optimal solvent density fluctuation

$$\delta\rho = -\frac{B_2c_k}{2B_3\bar{\rho}} \quad (25)$$

Substituting it back into eq 22, we obtain the free energy density

$$F \approx \frac{B_3\bar{\rho}^3}{3} + B_2\bar{\rho}c_k + \frac{c_k^2}{2}\left(k_BT\nu - \frac{B_2^2}{2B_3\bar{\rho}}\right) \approx \frac{B_3\bar{\rho}^3}{3} + B_2\bar{\rho}c_k + RT\frac{A_2}{2}c^2 \quad (26)$$

where $R = k_BN_{av}$ is the gas constant.

The solution concentration c can be expressed in terms of the number density of Kuhn segment c_k as

$$c = \frac{M_0}{N_{av}}c_k \quad (27)$$

Thus, polymer−solvent interactions lead to an effective second virial coefficient in the θ-region

$$A_2 \approx \frac{\nu N_{av}}{M_0^2}\left(1 - \frac{B_2^2}{2k_BT\nu B_3\bar{\rho}}\right) = \frac{\nu N_{av}}{M_0^2}\left(1 - \frac{\theta}{T}\right) \quad (28)$$

that vanishes at the theta temperature

$$\theta = \frac{B_2^2}{2k_B\nu B_3\bar{\rho}} \quad (29)$$

Thus, we derived that θ-temperature is inversely proportional to the average solvent density

$$\theta = \frac{\text{const}}{\bar{\rho}} \quad (30)$$

We have verified this dependence and found the value of the constant 260 g K/mL (eq 17) in our experiments. Substituting the second virial coefficient A_2 (eq 28) into eq 13, and using an estimation $\nu \approx db^2$ for the excluded volume of the rod of the length b and the effective diameter d, we find that $C_T^{A_2} \approx \nu/b^3 \approx d/b$. Therefore, we conclude that the coefficient $C_T^{A_2}$ is not universal, and it depends on chemical structure of the polymer in question. The effective diameter d and the Kuhn length b for PS are 8 Å and 18 Å, respectively. The effective diameter of the PFOMA is calculated to be 10 Å using the mass of Kuhn segment M_s, Kuhn length b (Table 2), and polymer density 2 g/cm^3. The ratio of d/b for PS and PFOMA is 0.44 and 0.33, and we find that $(d/b)_{PFOMA}/(d/b)_{PS} = 0.75$. This simple theoretical estimate is in good agreement with experimentally observed ratio$(C_T^{A_2})_{PFOMA}/(C_T^{A_2})_{PS} = 0.78 \pm 0.07$.

V. Conclusions

We have investigated the solution properties of a fluorinated poly(alkyl methacrylate) using both static and dynamic light scattering. The solvent quality of CO_2 was shown to improve with increasing temperature or CO_2 density. This trend was confirmed by the evaluation of the second virial coefficient A_2 measured by static light scattering. The θ-conditions were found as [$\theta = 27 \pm 1$ °C, $\rho_\theta = 0.86$ g/mL] and [$\theta = 25$ °C, $\rho_\theta = 0.88 \pm 0.02$ g/mL].

Both the hydrodynamic radius expansion factor and the normalized second virial coefficient of PFOMA dissolved in CO_2 are verified to be functions of the interaction parameter z, which is proportional to $N^{1/2}[1 - \theta(\rho)/T]$ (see eq 11), which is in excellent agreement with the data for other polymers dissolved in traditional organic solvents. We have for the first time demonstrated that the hydrodynamic radius expansion factor α_h and the normalized second virial coefficient are also functions of the same interaction parameter z and are proportional to the reduced solvent density $N^{1/2}[1 - \rho_\theta(T)/\rho]$ at constant temperature. We have determined and theoretically justified reciprocal dependence of the theta temperature on CO_2 density for PFOMA as $\theta(\rho) = (260/\rho)$(g K/mL). These results provide an important explanation of the observation that the solvent quality can be tuned by not only the solvent temperature but also the solvent density in a universal way.

We have also established that the hydrodynamic radius expansion factor can be expressed as a single function of the normalized second virial coefficient, independently of the methods used to vary the solvent quality.

$$\alpha_h = 1 + \frac{C^R}{C^{A_2}}A_2M_w^{1/2}\frac{M_0^{3/2}}{N_{av}b^3}$$

Note that coefficients $C^R/C^{A_2} = 0.12 \pm 0.02$ for PFOMA in CO_2 and 0.2 ± 0.03 for PS and PMMA solutions. The nonuniversality of the ratio of coefficients C^R/C^{A_2} indicates the existence of additional physical interactions that were not considered in existing polymer models. These interactions depend on chemical structure of polymers and will be discussed in our future publications.[38]

Acknowledgment. We thank the Kenan Center for the Utilization of Carbon Dioxide in Manufacturing and the NSF Science and Technology Center for Environmentally Responsible Solvents and Process (No. CHE-9876674) for financial support.

Supporting Information Available: Experimental details. This material is available free of charge via the Internet at http://pubs.acs.org.

References and Notes

(1) DeSimone, J. M.; Guan, Z.; Elsbernd, C. S. *Science* **1992**, *257*, 945−947.
(2) Quinn, E. L.; Jones, C. L. *Carbon Dioxide*; Reinhold Publishing Corp.: New York, 1936.

(3) McHugh, M. A.; Krukonis, V. J. *Supercritical Fluid Extraction: Principles and Practice*, 2nd ed.; Butterworth-Heineman: Stoneham, 1993.
(4) O'Neill, M. L.; Cao, Q.; Fang, R.; Johnston, K. P.; Wilkinson, S. P.; Smith, C. D.; Kerschner, J. L.; Jureller, S. H. *Ind. Eng. Chem. Res.* **1998**, *37*, 3067−3079.
(5) Garg, A.; Gulari, E.; Manke, C. W. *Marcromolecules* **1994**, *27*, 5643−5653.
(6) Tomasko, D. L.; Li, H.; Liu, D.; Han, X.; Wingert, M. J.; Lee, L. J.; Koelling, K. W. *Ind. Eng. Chem. Res.* **2003**, *42*, 6431−6456.
(7) DeSimone, J. M.; Maury, E. E.; Menceloglu, Y. Z.; Mcclain, J. B.; Romack, T. J.; Combes, J. R. *Science* **1994**, *265*, 356−359.
(8) Adamsky, F. A.; Beckman, E. J. *Macromolecules* **1994**, *27*, 312−314.
(9) Dillow, A. K.; Yun, S. L.; Suleiman, D. S.; Boatright, D. L.; Liotta, C. L.; Eckert, C. A. *Ind. Eng. Chem. Res.* **1996**, *35*, 1801−1806.
(10) Johnston, K. P.; Harrison, K. L.; Clarke, M. J.; Howdle, S. M.; Heitz, M. P.; Bright, F. V.; Carlier, C.; Randolph, T. W. *Science* **1996**, *271*, 624−626.
(11) Randolph, T. W. *Trends Biotechnol.* **1990**, *8*, 78.
(12) McAllister, K.; Sazani, P.; Adam, M.; Cho, M. J.; Rubinstein, M.; Samulski, R. J.; DeSimone, J. M. *J. Am. Chem. Soc.* **2002**, *124*, 15198−15207.
(13) Lemert, R. M.; Johnston, K. P. *Ind. Eng. Chem. Res.* **1991**, *30*, 1222.
(14) Mertsch, R.; Wolf, B. A. *Macromolecules* **1994**, *27*, 3289−3294.
(15) Cotts, P. M. *Macromolecules* **1994**, *27*, 6487−6491.
(16) Fulton, J. L.; Pfund, D. M.; McClain, J. B.; Romack, T. J.; Maury, E. E.; Combes, J. R.; Samulski, E. T.; DeSimone, J. M.; Capel, M. *Langmuir* **1995**, *11*, 4241−4249.
(17) Guan, Z. Department of Chemistry, University of North Carolina, Chapel Hill, 1994.
(18) Chu, B.; Lin, J. S. *J. Chem. Phys.* **1970**, *53*, 4454.
(19) Nagashima, K.; Lee, C. T.; Xu, B.; Johnston, K. P.; DeSimone, J. M.; Johnson, C. S. *J. Phys. Chem. B* **2003**, *107*, 1962−1968.
(20) Folk, S. L. Department of Chemistry, University of North Carolina, Chapel Hill, 2003.
(21) Buhler, E.; Dobrynin, A. V.; DeSimone, J. M.; Rubinstein, M. *Macromolecules* **1998**, *31*, 7347−7355. McClain, J. B.; Londono, D.; Combes, J. R.; Romack, T. J.; Canelas, D. A.; Betts, D. E.; Wignall, G. D.; Samulski, E. T.; DeSimone, J. M. *J. Am. Chem. Soc.* **1996**, *118*, 917−918.
(22) Wignall, G. D.; Melnichenko, Y. B.; Triolo, R.; McClain, J. B.; DeSimone, J. M. *Abstr. Pap. Am. Chem. Soc.* **2001**, *221*, U374−U375.
(23) ChilluraMartino, D.; Triolo, R.; McClain, J. B.; Combes, J. R.; Betts, D. E.; Canelas, D. A.; DeSimone, J. M.; Samulski, E. T.; Cochran, H. D.; Londono, J. D. *J. Mol. Struct.* **1996**, *383*, 3−10.
(24) Huglin, M. B. *J. Appl. Polym. Sci.* **1965**, *9*, 3963−4001, 4003−4024.
(25) Burns, R. C.; Graham, C.; Weller, A. R. M. *Mol. Phys.* **1986**, *59*, 41−64.
(26) Chu, B. *Laser Light Scattering: Basic Principles and Practice*, 2nd ed.; Academic Press: Boston, 1991.
(27) Yamakawa, H. *Modern Theory of Polymer Solutions*; Harper and Row: New York, 1970.
(28) Berry, G. C. *J. Chem. Phys.* **1966**, *44*, 4550−4564.
(29) Rubinstein, M.; Colby, R. H. *Polymer Physics*; Oxford University Press: New York, 2003.
(30) Schulz, G. V.; Inagaki, H.; Kirste, R. *Z. Phys. Chem. (Munich)* **1960**, *24*, 290−404.
(31) Arai, T.; Abe, F.; Yoshizaki, T.; Einaga, Y.; Yamakawa, H. *Macromolecules* **1995**, *28*, 3609−3616.
(32) Arai, T.; Abe, F.; Yoshizaki, T.; Einaga, Y.; Yamakawa, H. *Macromolecules* **1995**, *28*, 5458−5464.
(33) Melnichenko, Y. B.; Kiran, E.; Heath, K. D.; Salaniwal, S.; Cochran, H. D.; Stamm, M.; Van Hook, W. A.; Wignall, G. D. *J. Appl. Crystallogr.* **2000**, *33*, 682−685.
(34) Nose, T.; Chu, B. *Macromolecules* **1979**, *12*, 1122−1129.
(35) Chu, B.; Nose, T. *Macromolecules* **1980**, *13*, 122−132.
(36) Konishi, T.; Yoshizaki, T.; Saito, T.; Einaga, Y.; Yamakawa, H. *Macromolecules* **1990**, *23*, 290−297.
(37) Mitsuo, N. *Phys. Rev. E* **1995**, *51*, 5770.
(38) Panyukov, S.; Shirvanyants, D.; Liao, Q.; Rubinstein, M., to be published.
(39) Akcasu, A. Z. *Polymer* **1981**, *22*, 1169−1180.

MA052409K